

Numerical Simulation of the Combustion of PETN/TNT Products with Air in Closed Chambers

John B. Bell, Marcus Day, Vincent Beckner, Charles Rendleman
University of California Lawrence Berkeley National Laboratory,
Berkeley, CA USA

Allen L. Kuhl*
University of California Lawrence Livermore National Laboratory,
Livermore, CA USA

P. Neuwald
Ernst-Mach-Institut, Fraunhofer Institut für Kurzzeitdynamik,
Freiburg im Breisgau, Germany

1 Introduction

For many explosives, only a fraction of the chemical energy is released in the detonation. Calorimetry data for TNT from Ornellas [8] shows that when the ambient gas is inert, there is substantially less total energy released than when the ambient gas is air. This data indicates that burning of the explosion byproducts plays a key role in the overall energetics of the system. The basic concept of shock-dispersed fuel (SDF) charges is to directly exploit this idea. More precisely, in an SDF charge a small charge is used to disperse a fuel and create a turbulent environment in which the fuel can mix with ambient air and burn.

Here, we consider a prototype SDF charge in which a 0.5 g PETN booster charge is used to disperse 1.0 g of TNT which plays the role of the fuel [6]. The hot detonation products and dispersed material are rich in fuel ($C_{(s)}$, CO and H_2), and when they mix with air and burn, they release 2,500 cal/g (in addition to the 1,100 cal/g released by the detonation) in a non-premixed turbulent combustion process [3]. The goal in this paper is to explore the dependence of the total energy release on the geometry of the calorimeter. As a baseline case, we consider a charge in air in a 6.6 l calorimeter [6]. We first present two simulations of this baseline case corresponding to filling the calorimeter with air and filling the calorimeter with an inert gas. Comparison of these two cases illustrates the role of burning on the overall system energetics. We then discuss two series of simulations focused on exploring the dependence of the system response on problem geometry. In the first set of simulations, the aspect ratios of the calorimeter are held constant but the volume is increased. In the second set the volume is held constant but the aspect ratios are changed. In the next two sections, we briefly discuss the computational model and the numerical method used for the simulations. In the final section we present the computational results and discuss the implications of the results to the design of SDF charges.

*Corresponding author, Allen Kuhl, kuhl2@llnl.gov

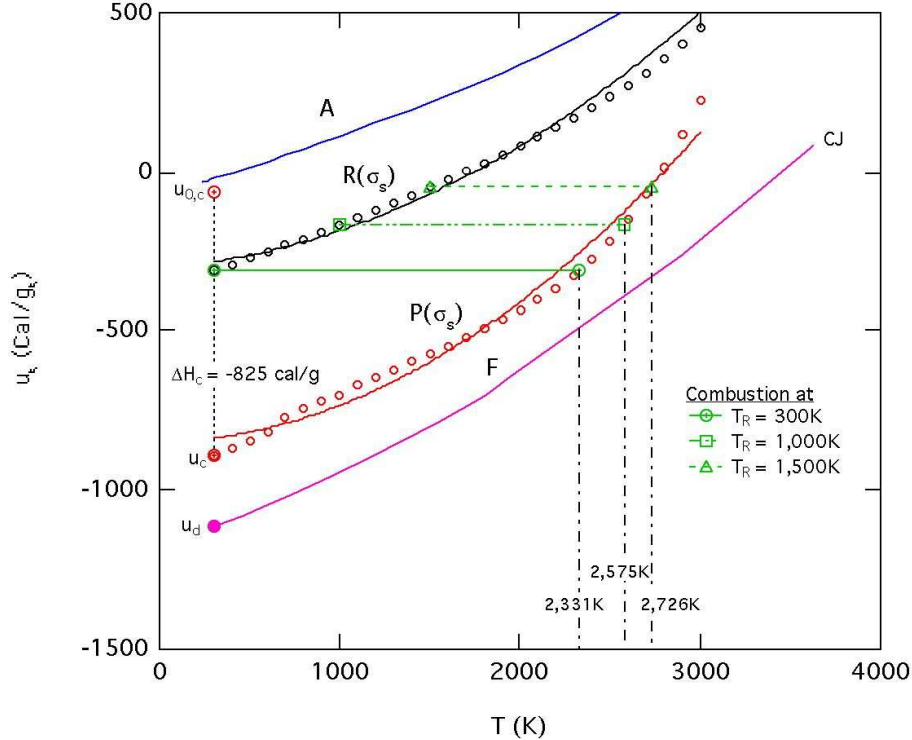


Figure 1: Locus of states in the Le Chatelier diagram for stoichiometric combustion ($\sigma_s = 2.773$) of the explosion products from the composite (PETN/TNT) charge in the 6.6 l calorimeter. The green lines illustrate combustion loci starting at 300 K, 1000 K and 1500 K. EOS curves are: $u_A(T) = 1.86 \cdot 10^{-5}T^2 + 0.167 \cdot T - 72.2 \text{ cal/g}_A$, $u_F(T) = 4.59 \cdot 10^{-5}T^2 + 0.179 \cdot T - 1168 \text{ cal/g}_F$, $u_P(T) = 10.5 \cdot 10^{-5}T^2 + 0.1111 \cdot T - 848 \text{ cal/g}_P$, $u_R(T) = 7.56 \cdot 10^{-5}T^2 + 0.042 \cdot T - 302 \text{ cal/g}_R$. Here, the label $R(\sigma_s)$ and $P(\sigma_s)$ emphasizes that the reactants and products were computed for a stoichiometric mixture of fuel and air.

2 Thermodynamic model

Developing a computational model to simulate afterburning poses something of a conundrum. One possible approach would be include a collection of chemical reactions that would capture both the chemical behavior of the detonation products as the gases expand into the calorimeter and reactions describing the oxidation of those detonation products as they mix with air. The difficulty with this approach is that even if suitable reactions were known, the resulting computation would be extremely costly. Furthermore, much of the chemical detail is relatively unimportant because the chemical time scales are very fast because of the high temperature and pressure environment.

An alternative would be to attempt to enforce some type of chemical equilibrium assumption and perform a simulation in which it is assumed that the chemical constituents are always in chemical and thermal equilibrium. However, this approach fails to accurately predict the dynamics even in the inert case in which the calorimeter is filled with nitrogen. Data from Kuhl et al. [4] shows that an equilibrium assumption does not give an accurate picture of the composition of gases resulting from a TNT charge. In essence, as the gases expand the behind the detonation, the temperature

drops to the point that the reactions are effectively quenched.

Kuhl et al. [4] has developed a thermodynamic model that can accurately describe the behavior of the detonation products and provide a simplified model for the combustion process. This approach is based on a thermodynamics analysis in the Le Chatelier diagram of specific internal energy versus temperature shown in Figure 1. We note that, for these definitions, we include the chemical potential as part of the internal energy so that chemical reactions at constant volume do not change the internal energy. For this analysis we treat the gases as three components, fuel (the detonation products), air and products (the result of afterburning). The thermodynamic properties of the components k (Fuel-F, Air-A, and Products-P) were computed using the Cheetah code [2] by Kuhl et al. [4]. In addition, for convenience we denote the mixture of fuel and air as the Reactants-R. When constructing the thermodynamic properties of the detonation products, we assume that the detonation products are in chemical equilibrium above $T=1,800$ K at which point the composition is frozen. This assumption produces a good approximation to the bomb calorimeter data of Ornellas [8]. The resulting data is then fit with quadratics to establish the equation of state (EOS) of the components:

$$u_k(T_k) = a_k T_k^2 + b_k T_k + c_k, \quad (k = F, A, R, P)$$

These quadratic EOS functions (curves in Figure 1) well approximate the thermodynamic values (circles in Figure 1) and fully characterize the thermodynamic behavior of the system [4]. From these component EOS we can construct mixture thermodynamic properties based on an ideal gas approximation.

Mixture EOS:

$$T_m = [-b_m + \sqrt{b_m^2 - 4a_m(c_m - u_m)}] / 2a_m, \quad p_m = \rho_m R_m T_m$$

Mixture Properties:

$$a_m = \sum_k Y_k a_k, \quad b_m = \sum_k Y_k b_k, \quad c_m = \sum_k Y_k c_k, \quad R_m = \sum_k Y_k R_k$$

3 Gas Dynamics

We model the flow using the equations of inviscid, gas dynamics for the multi-component mixture m . Thus, the simulations implicitly incorporate a Monotone Integrated Large Eddy Simulation (MILES) type representation of mixing, described by Boris et al. [1], which is a reasonable approximation to the high Reynolds and Peclet numbers associated with the post-detonation environment. More precisely, we solve

Mass:

$$\partial_t \rho_m + \nabla \cdot (\rho_m u) = 0 \tag{1}$$

Momentum:

$$\partial_t \rho_m u + \nabla \cdot (\rho_m u u) = -\nabla p_m \tag{2}$$

Energy:

$$\partial_t \rho_m (u_m + u \cdot u / 2) + \nabla \cdot \rho_m (u_m + u \cdot u / 2) u = -\nabla \cdot (p_m u) \tag{3}$$

Components:

$$\partial_t Y_k + u \cdot \nabla Y_k = \alpha_k \dot{Y}_s, \quad \sum_k Y_k = 1 \tag{4}$$

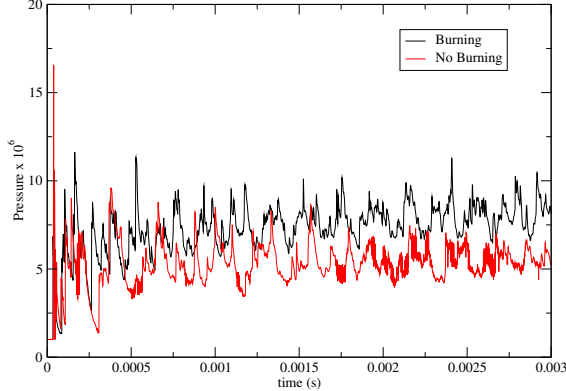


Figure 2: Pressure traces for configuration A showing the pressure enhancement due to afterburning of the products of the detonation.

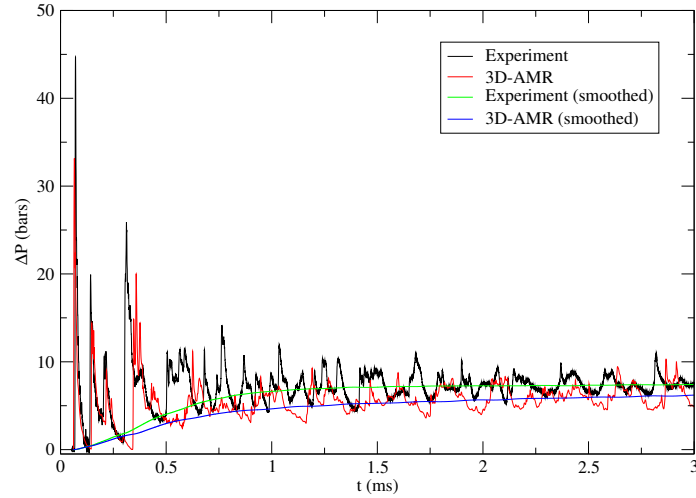
where ρ_m , u_m , and p_m are the mixture density, internal energy and pressure, u is the flow velocity, Y_k are the mass fractions, $k = F, A, P$ and $\alpha_k = \{-1, -\sigma_s, (1 + \sigma_s)\}$ denotes the stoichiometric source/sink coefficients based on the stoichiometric air/fuel ratio: $\sigma_s = 2.77$. The term \dot{Y}_s embodies chemical kinetic effects. Here it is assumed that reactions occur on a much faster time scale than the fluid mechanics; i.e., mixtures of fuel and air instantly react to products so that mixing controls the reaction process. In addition, as noted earlier, we use a MILES approach to represent the mixing; thus the simulation represents a large-Damkhöler-number and Reynolds number limit.

The above model equations (Equations 1–4) were integrated using a high-order Godunov scheme, and Adaptive Mesh Refinement (AMR) [10] was used to follow the thin reaction zones on the computational grid. The geometry of the calorimeter is represented using an embedded boundary representation. The overall computational method is discussed in Pember et al. [9].

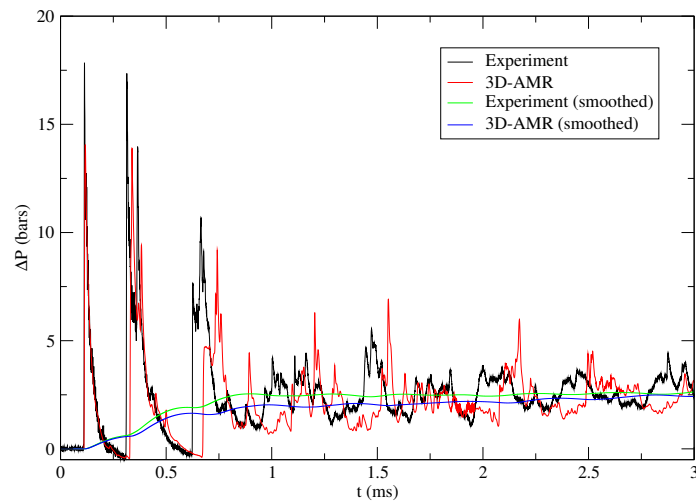
4 Results

The computations were performed in two stages. In the first stage, we simulated the initial explosion using a Jones-Wilkins-Lee (JWL) [5] equation of state to model the condensed phase behavior of the detonation products at early time. For this phase of the computation, three levels of refinement were used for an effective resolution of approximately 0.4 mm. After the initial charge has expanded to three charge radii, the behavior is well approximated by an ideal gas. At that point, we switch to the quadratic thermodynamic model discussed above. We then also reduce the effective resolution to 0.8 mm for the remainder of the simulation.

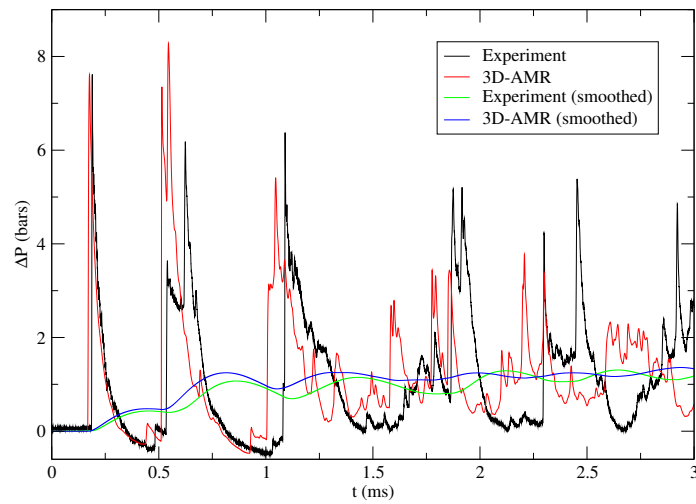
Computations were performed for five cases listed in Table 1. The baseline case, A, is a circular cylinder with an aspect ratio $L/D=1$ and a volume of 6.6 liters. In Figure 2 we present pressure traces from simulations with and without afterburning. These traces illustrate the enhancement to the pressure load resulting from the energy released by combustion of the detonation products. Cases B and C, are also circular cylinders with the same aspect ratio but of volumes 21.2 and 40.5 liters, respectively. These cases explore the effect of chamber volume on the efficiency of the turbulent combustion process. In cases A, D, and E, the chamber volume was fixed (6.3–6.6 liters), and the chamber aspect ratio was varied: $L/D=1, 4.6$ and 12.5 , respectively. These latter cases explore the effect of lateral confinement (tube walls) on the combustion process.



Case A

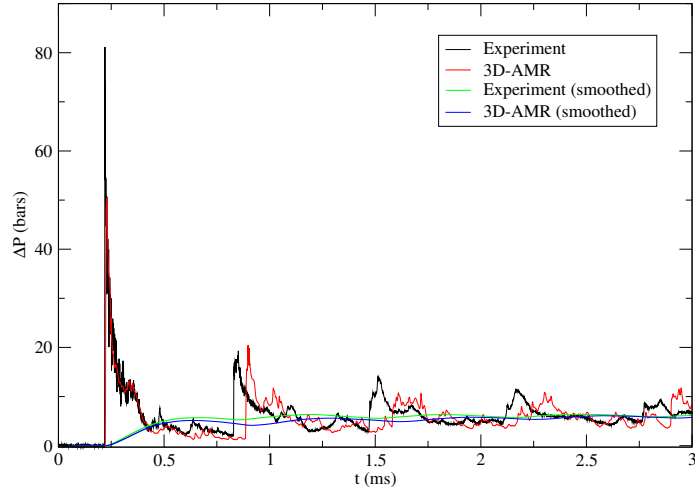


Case B

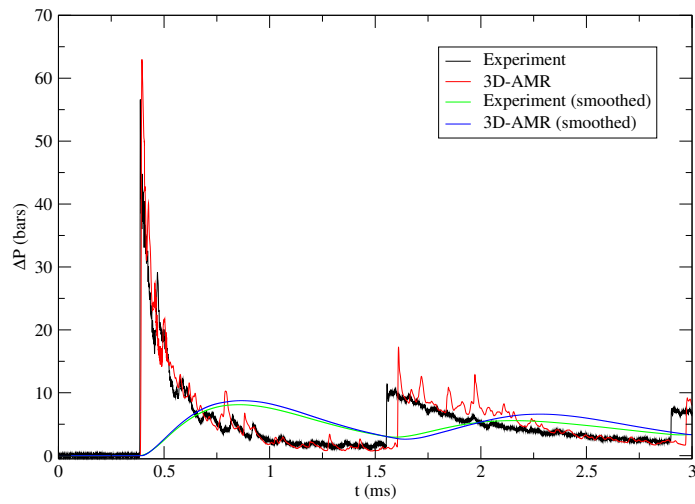


Case C

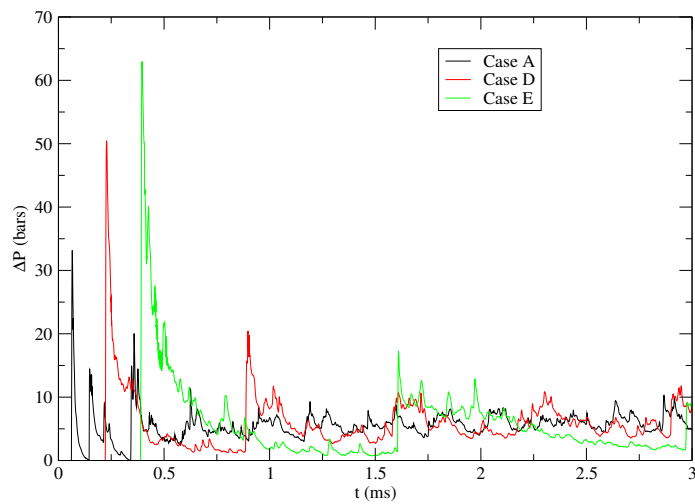
Figure 3: Comparison of pressure histories from numerical simulations with experimental data for explosion of 1.5 g PETN/TNT charges in cylindrical ($L/D=1$) chambers of different volumes (Case A: 6.6 liter; Case B: 21.5 liter; Case C: 40.5 liter).



Case D



Case E



Case A,D,E

Figure 4: Comparison of pressure histories from numerical simulations with experimental data for explosion of 1.5 g PETN/TNT charges in 6.6 liter chambers with different aspect ratios (Case A: $L/D=1$; Case D: $L/D=4.6$; and Case E: $L/D=12.5$).

Name	Symbol	Length (mm)	Diameter (mm)	cross- section	Volume (l)	L/D
BBC[6.6/1]	A	210	200	circular	6.6	1.05
BBC[21.2/1]	B	300	300	circular	21.2	1.00
BBC[40.5/1]	C	379	369	circular	40.5	1.03
BBC[6.3/4.6]	D	555	120	circular	6.3	4.625
BBC[6.3/12.5]	E	1000	80	square	6.3	12.5

Table 1: Summary of currently available barometric bomb calorimeters

Experiments were performed in chambers A–E; pressure histories were recorded on the end wall of the cylinder or tube [7]. Results of the numerical simulations are compared with these measured pressure records in Figures 3 and 4. There is excellent agreement between computation and experiment on the initial shock arrival and pressure profile behind the initial shock front, indicating that the numerical model has the correct amount of energy in the charge to drive the blast wave in the air. At intermediate times (i.e., second and third blast waves), the computed shock arrival times also agree with measurements, proving that computed turbulent combustion cloud has the right temperature/sound speed, in other words, the combustion rate in the simulation is similar to that found in the experiments. At later times, turbulence influences the pressure waves; even gauges at the same slant range from the charge measure different acoustic signals. Nevertheless, the measured and computed pressures profiles have similar mean values at late times as shown in the filtered traces in Figures 3 and 4. These smoothed records suggest that the fuel consumed in the numerical simulation is representative of that found in the experiment. (We note that for Case A, we predict somewhat lower pressure than was measured in the experiment suggesting an underestimate of the combustion process in this case. We are currently exploring the mechanism for this reduction.)

The computed fuel histories are presented in Figure 5. In the L/D=1 chambers (cases A, B and C), there was 0.4–0.5 g (or 27–35% of the 1.5 g) of fuel remaining after 3 ms. Thus about 70% of the fuel mass was consumed by combustion during 3 ms. In addition, the temporal history of the overall combustion process is quite similar. The fuel history to the higher aspect ratio cases is more interesting. For the moderate aspect ratio case, D, the combustion process starts more slowly than in case A but catches up by 3 ms. In the large aspect ratio case, E, only about 0.5 g (33%) of the fuel has been consumed during 3 ms and the fuel consumption rate has flattened considerably. This suggests that the walls in case E limit the ability of turbulent mixing to bring fuel and oxidizer together.

This is illustrated graphically in Figure 6 which provides a slice through the center of the chamber showing the distribution of fuel, oxidizer and products in the system. From the figure one can see that combustion products gases form a protective layer that separates the fuel (in the center of the tunnel) from the air (near the ends of the tunnel). Thus, in case E the geometry of the chamber introduces a significant constraint on the afterburning process.

5 Summary

The detonation products resulting from a chemical explosion are typically not completely oxidized and will burn if mixed with oxygen at sufficiently high temperature. In this paper we have presented

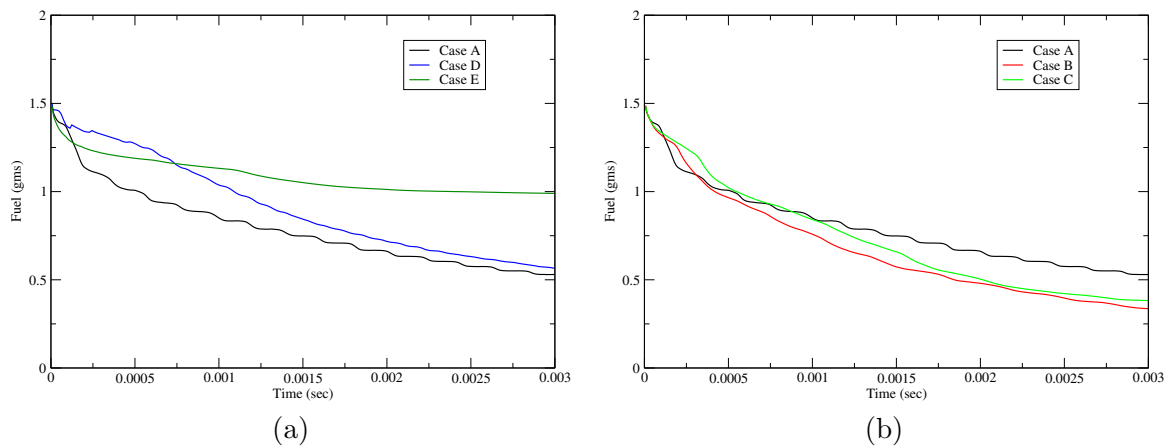


Figure 5: (a) Integrated fuel histories for fixed combustor volume but changing combustor geometry, corresponding to cases A, D, and E in Table 1. (b) Integrated fuel histories for fixed geometry but increasing combustor volume corresponding to cases A, B, and C in Table 1.

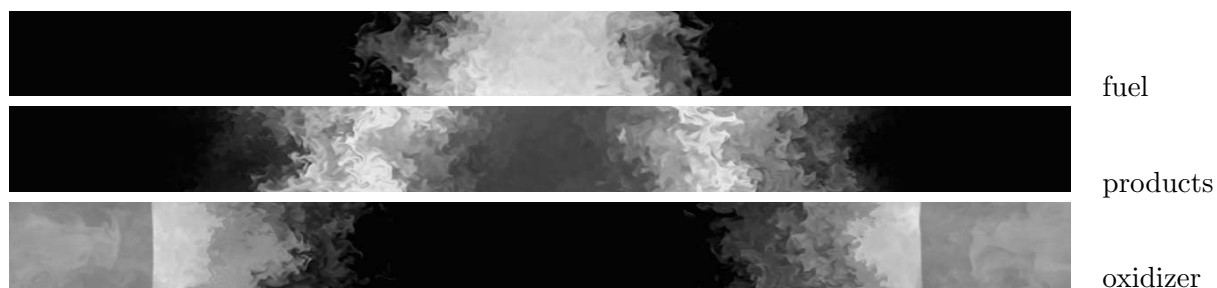


Figure 6: Fuel, products and oxidizer concentrations for case E, showing the products segregate the fuel from the oxidizer

a computational model for the afterburning of these detonation products based on a thermodynamic model developed by Kuhl. This model captures much of the thermodynamic and chemical behavior of the detonation products as they expand after detonation and provides a thermodynamically and chemically consistent model for their subsequent oxidation. The thermodynamic model is incorporated into a three-dimensional AMR algorithm and used to study the behavior of a composite TNT/PETN charge in a calorimeter. For the cases considered here, this approach has allowed us to obtain a good match to experimental data for several different chamber geometries suggesting that this approach is adequate to capture the dominant energetics of afterburning. In future work, we shall continue with additional validation studies of this approach and extend the methodology to consider alternative fuels to be dispersed by the initial blast wave. In addition, we will continue to explore the role of system geometry on the overall combustion process.

References

- [1] J. Boris, F. Grinstein, E. Oran, and R. Kolbe. New insights into large eddy simulation. *Fluid Dynamics Research*, 10, 1992.
- [2] Laurence E. Fried, P.C. Souers, W.M Howard, and P. Vitello. LLNL CHEETAH Code. <http://www-cms.llnl.gov/s-t/cheetah.html>.
- [3] A. L. Kuhl, R. E. Ferguson, and A. K. Oppenheim. Gasdynamics of combustion of TNT products in air. *Archivum Combustionius*, 19(1–4):67–89, 1999.
- [4] A. L. Kuhl, M. Howard, and L. Fried. Thermodynamic model of afterburning in explosions. *Energetic Materials, 34th ICT Conference*, pages 74.1–74.14, 2003.
- [5] E. Lee, M. Finger, and W. Collins. JWL equation of state coefficients for high explosives. Technical Report UCID-16189, Lawrence Livermore National Laboratory, Livermore, CA, 1973.
- [6] P. Neuwald, H. Reichenbach, and A. L. Kuhl. Shock-dispersed fuel charges combustion in chambers and tunnels. *Energetic Materials, 34th ICT Conference*, pages 13.1–13.14, 2003.
- [7] P. Neuwald, H. Reichenbach, and A. L. Kuhl. Shock-dispersed fuel charges combustion in chambers and tunnels. *ICDERS-19, Hakone, Japan*, 2003.
- [8] D. L. Ornellas. Calorimetric determination of the heat and products of detonation for explosives: October 1961 to April 1982. Technical Report UCRL-52821, Lawrence Livermore National Laboratory, Livermore, CA, 1984.
- [9] R.B. Pember, J.B. Bell, P. Colella, W.Y. Crutchfield, and M.L. Welcome. An adaptive cartesian grid method for unsteady compressible flow in irregular regions. *J. Comp. Phys.*, 120(2):278–304, September 1995.
- [10] Charles A. Rendleman, Vincent E. Beckner, Mike Lijewski, William Y. Crutchfield, and John B. Bell. Parallelization of structured, hierarchical adaptive mesh refinement algorithms. *Computing and Visualization in Science*, 3(3):147–157, 2000.